CORE
Metadata, citation and similar papers at core.ac.uk
Provided by NASA Technical Reports Server

(NASA-CR-142262) ANALYSIS OF OSO DATA TO DETERMINE THE STRUCTURE AND ENERGY BALANCE OF THE SOLAR CHROMOSPHERE (Smithsonian Astrophysical Observatory) 26 p HC $3.75 CSCL 03B G3/92
N75-20190
Unclas
13433

ANALYSIS OF OSO DATA TO DETERMINE THE STRUCTURE AND ENERGY BALANCE OF THE SOLAR CHROMOSPHERE

Grant NGR 09-015-210

Final Report

Principal Investigators

Dr. Eugene H. Avrett
Dr. Wolfgang Kalkofen

February 1975

Prepared for

National Aeronautics and Space Administration
Washington, D.C. 20546

RECEIVED
NASA STI FACILITY
INPUT BRANCH
APR 1975

Smithsonian Institution
Astrophysical Observatory
Cambridge, Massachusetts 02138

The Smithsonian Astrophysical Observatory
and the Harvard College Observatory
are members of the
Center for Astrophysics

ANALYSIS OF OSO DATA TO DETERMINE THE STRUCTURE AND ENERGY BALANCE OF THE SOLAR CHROMOSPHERE

Grant NGR 09-015-210

Final Report

Principal Investigators

Dr. Eugene H. Avrett
Dr. Wolfgang Kalkofen

February 1975

Prepared for
National Aeronautics and Space Administration
Washington, D.C. 20546

Smithsonian Institution
Astrophysical Observatory
Cambridge, Massachusetts 02138

The Smithsonian Astrophysical Observatory
and the Harvard College Observatory
are members of the
Center for Astrophysics

503-060

ANALYSIS OF OSO DATA TO DETERMINE THE STRUCTURE AND ENERGY BALANCE OF THE SOLAR CHROMOSPHERE

Grant NGR 09-015-210

The objectives of the research supported by this grant are twofold:

1) The determination of an improved empirical model of the temperature-density structure of the solar atmosphere based on OSO 4 and 6 data, and

2) The determination of an associated theoretical model based on radiative balance, thermal conduction, and shock heating.

The following work has been performed to accomplish these objectives.

We have carried out a detailed reexamination of the temperature-density structure of the photosphere and low chromosphere. The middle and upper chromosphere, which directly emits most of the OSO spectrum, is sensitive to conditions in this underlying region of the atmosphere. Our model of this region is based on a unified compilation of all recently published broadband flux and central intensity observations of the solar spectrum from 500 μm in the far infrared to 1220 Å in the far ultraviolet. This extensive compilation includes the OSO 4 and 6 observations in the wavelength range 1400 to 1220 Å. A complete report on this work by Vernazza, Avrett, and Loeser has been widely distributed in preprint form and will appear in <u>The Astrophysical Journal Supplement Series</u>.

We have also calculated a new model of the quiet solar atmosphere in the height range between the temperature minimum and the upper part of the chromosphere–corona transition region. This model is based on statistical equilibrium calculations of H, He I, He II, Si I, C I, and other ions. The results of these calculations will appear in forthcoming papers to be submitted to <u>The Astrophysical Journal.</u>

Finally, we have studied the propagation and dissipation of acoustic waves in the solar atmosphere and the dependence of the dissipation on the energy flux and the period of the waves. We conclude that the low chromosphere is heated by short-period waves. An account of this work was presented by Kalkofen at a recent solar physics meeting of the American Astronomical Society. The text of that paper follows as Appendix A.

In addition, we reproduce in Appendix B the text of the paper "Formation of the Solar EUV Spectrum," presented by Avrett at the same meeting.

APPENDIX A

HEATING OF THE LOW SOLAR CHROMOSPHERE

Wolfgang Kalkofen

Center for Astrophysics
Harvard College Observatory and Smithsonian Astrophysical Observatory
Cambridge, Massachusetts 02138

and

Peter Ulmschneider

University of Würzburg
Würzburg, Germany

Presented at
the Fifth Meeting of the Solar Physics Division
American Astronomical Society
January 19–23, 1975
University of Colorado, Boulder, Colorado

HEATING OF THE LOW SOLAR CHROMOSPHERE

Wolfgang Kalkofen and Peter Ulmschneider

INTRODUCTION

The temperature of the solar atmosphere decreases monotonically from the interior to the height of the temperature minimum and then rises again into the chromosphere and corona. This temperature rise is due to nonradiative energy input into the chromosphere. Biermann (1948) and Schwarzschild (1948) have suggested that the energy that heats the chromosphere is carried in mechanical waves that are generated in the convection zone and dissipate their energy in the chromosphere. Osterbrock (1961) has estimated the flux, and Stein (1968) has calculated frequency spectra of the acoustic waves. In this paper, we want to study the propagation and dissipation of acoustic waves in the solar atmosphere and the dependence of the dissipation on the energy flux and on the period of the waves.

Observations place two constraints on the energy flux and the period of the waves: They must be such that the height at which the sound waves steepen into shocks and dissipate a large fraction of their energy agrees with the location of the temperature minimum and that the energy flux remaining in the waves thereafter is sufficient to account for the radiative losses of the chromosphere.

The theory of wave generation gives the energy flux and the spectrum. These calculated quantities are very uncertain because of the dependence of the flux on the eighth power of the velocities in the convection zone, which are only poorly determined from mixing-length theory. Osterbrock (1961) has determined a value for the noise flux of 3×10^7 ergs/cm^2 sec; Stein's (1968) value is slightly larger. For several turbulence spectra, Stein has calculated the corresponding noise spectra, which show broad maxima with periods between 20 and 80 sec.

The dissipation of sound waves in the low chromosphere has been studied by Ulmschneider (1970). He has concluded that the low chromosphere must be heated by short-period waves whose periods are on the order of 30 sec. This conclusion is supported by Stein's spectrum of the acoustic flux. It is not supported by observations, but there are also no observations that would rule out heating by short-period waves.

Acoustic waves with periods near 30 sec and an initial energy flux of 3×10^7 ergs/ cm^2 sec at the bottom of the photosphere dissipate their energy just beyond the temperature minimum region. Waves with longer periods, and therefore longer wavelengths, travel farther into the chromosphere before they dissipate, and waves with a shorter period dissipate earlier. If waves with periods much below 30 sec carried enough energy, they would cause the chromospheric temperature rise at lower depth; and thus the temperature minimum would lie at a lower depth, contrary to observation.

RESULTS

We have solved the time-dependent hydrodynamic equations for a plane-parallel model of the solar atmosphere, using the method of characteristics. Radiative damping by means of emission and absorption in H^- was taken into account. The numerical solutions gave the height where the waves steepen into shocks and dissipate most of their energy and the amount of energy that remains in the wave after shock formation.

The temperature of two models of the solar atmosphere is shown as a function of the optical depth at 5000 Å in Figure 1. The theoretical model in radiative equilibrium was constructed by Kurucz (1974). Its temperature decreases monotonically with height. The empirical model, the so-called HSRA (Gingerich et al., 1971), was designed to reproduce the observations of the photosphere and the chromosphere. Its temperature drops through the photosphere to the temperature minimum and then rises again into the chromosphere and corona. The temperature at the minimum is approximately 4000 K, where the optical depth is $\tau_{5000} = 10^{-4}$ and the height above $\tau_{5000} = 1$ is h = 550 km.

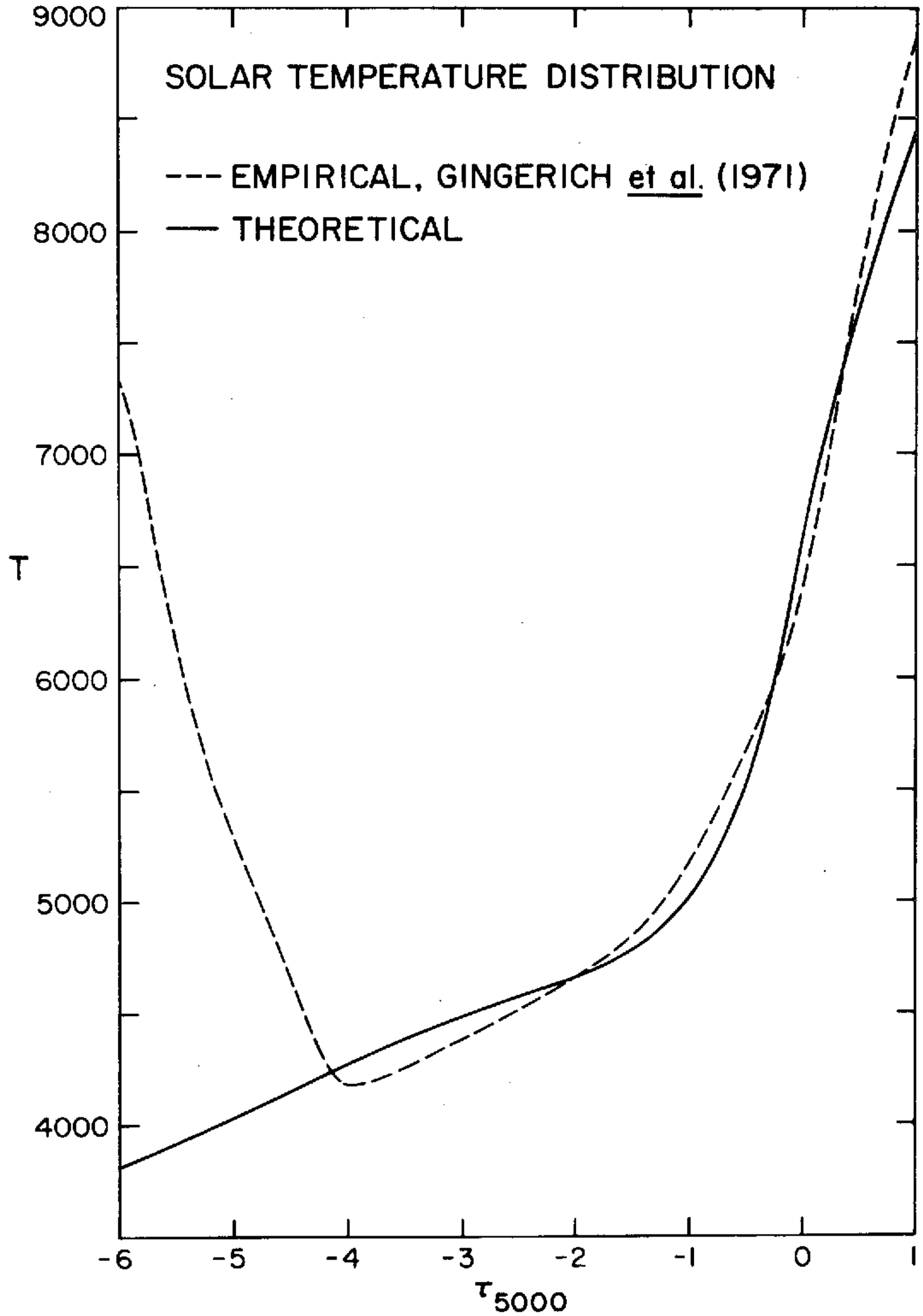

Figure 1. The temperature T of the solar atmosphere as a function of τ_{5000}.

We have taken the static model atmosphere by Kurucz (1974) and have excited at its bottom a sound wave. The initial energy flux is that from Osterbrock (3×10^7 ergs/cm^2 sec), the wave period is 25 sec, the wavelength at the lower temperatures is 180 km, and the scale height is 120 km. The initial velocity amplitude is 0.05 km/sec, and where the sound wave has steepened into a shock the wave velocity has reached 1 km/sec (Figure 2). Note that the sound velocity at that point is 7 km/sec. Thus, the shock is weak, and its Mach number is $M = 1.13$.

The shock occurs at a height of $h = 650$ km. This point defines the beginning chromospheric temperature rise and thus the location of the temperature minimum. The wave dissipates 90% of its energy at the shock and then continues with reduced amplitude, carrying the remaining 10% of its energy farther into the chromosphere.

The temperature of the static atmosphere and the temperature perturbation caused by the wave scaled up by a factor of 10 are shown in Figure 3. At the shock front, the temperature perturbation reaches an amplitude of 500 K.

The height of shock formation is shown as a function of the wave period and the initial energy in Figure 4. "HSRA observed" refers to the location of the temperature minimum in the empirical model. We see that, generally, the height where the shock forms increases with increasing period on wavelength, as expected. The increase in the height for short-period waves may be caused by the greater efficiency of radiative damping when the distance between wave maxima and minima is small; or we may be reading too much into these preliminary results. The "best" initial energy is 3×10^7 ergs/cm^2 sec. The temperature minimum for a 30-sec wave with this energy lies at 650 km, nearly one scale height higher than it does in the empirical HSRA. But this higher location may be in better accord with center-to-limb observations of solar radiation at long wavelengths.

The wave energy carried beyond the point of shock formation is shown as a function of wave period and initial energy in Figure 5. "HSRA" refers to the radiative flux emitted by the chromosphere in H^- and in certain lines as determined by Athay (1970) and by others. We see that the agreement with observations is good for an initial energy flux of 3×10^7 ergs/cm^2 sec and wave periods near 30 sec.

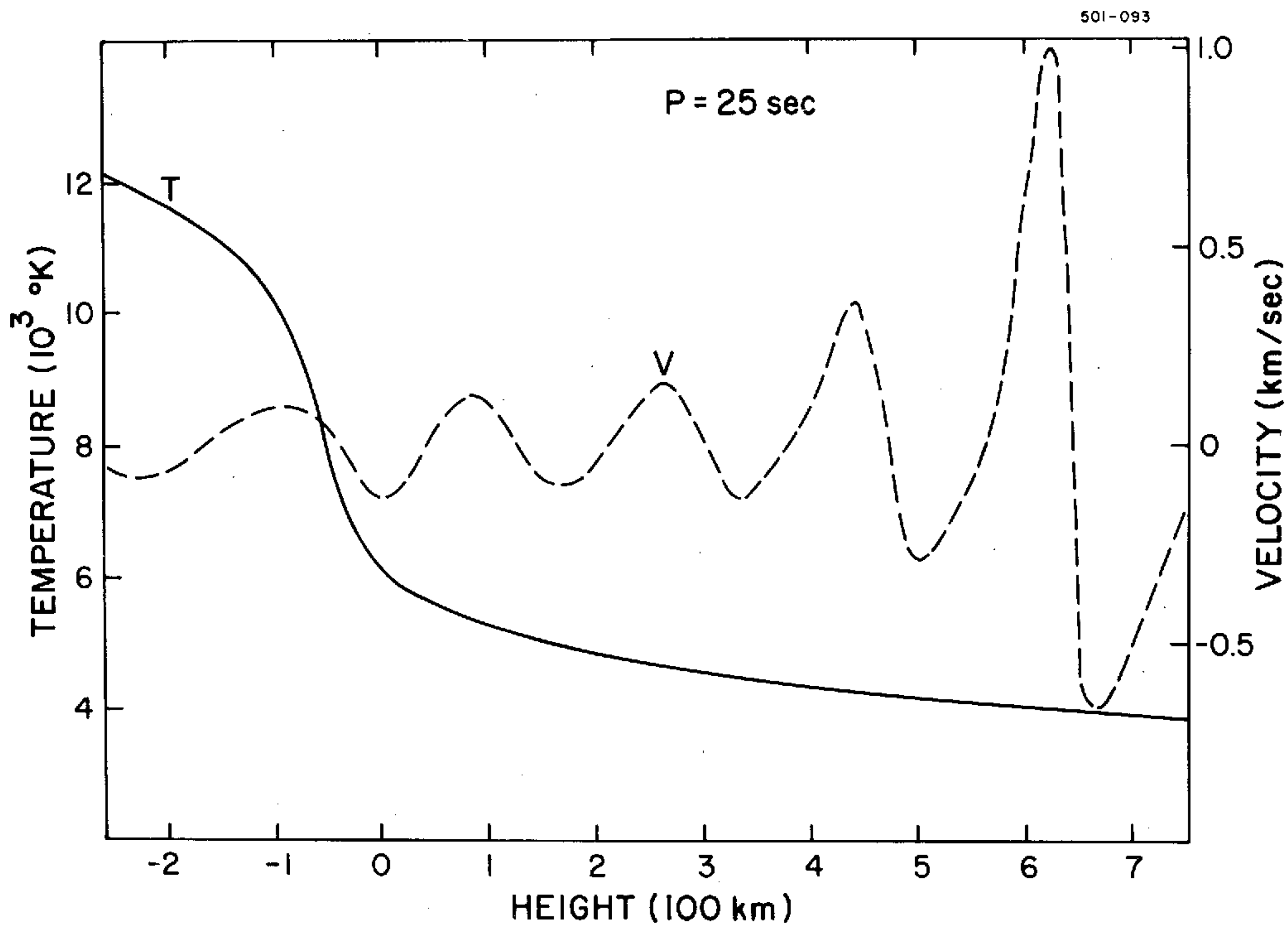

Figure 2. Temperature T and wave amplitude v as functions of height above $\tau_{5000} = 1$.

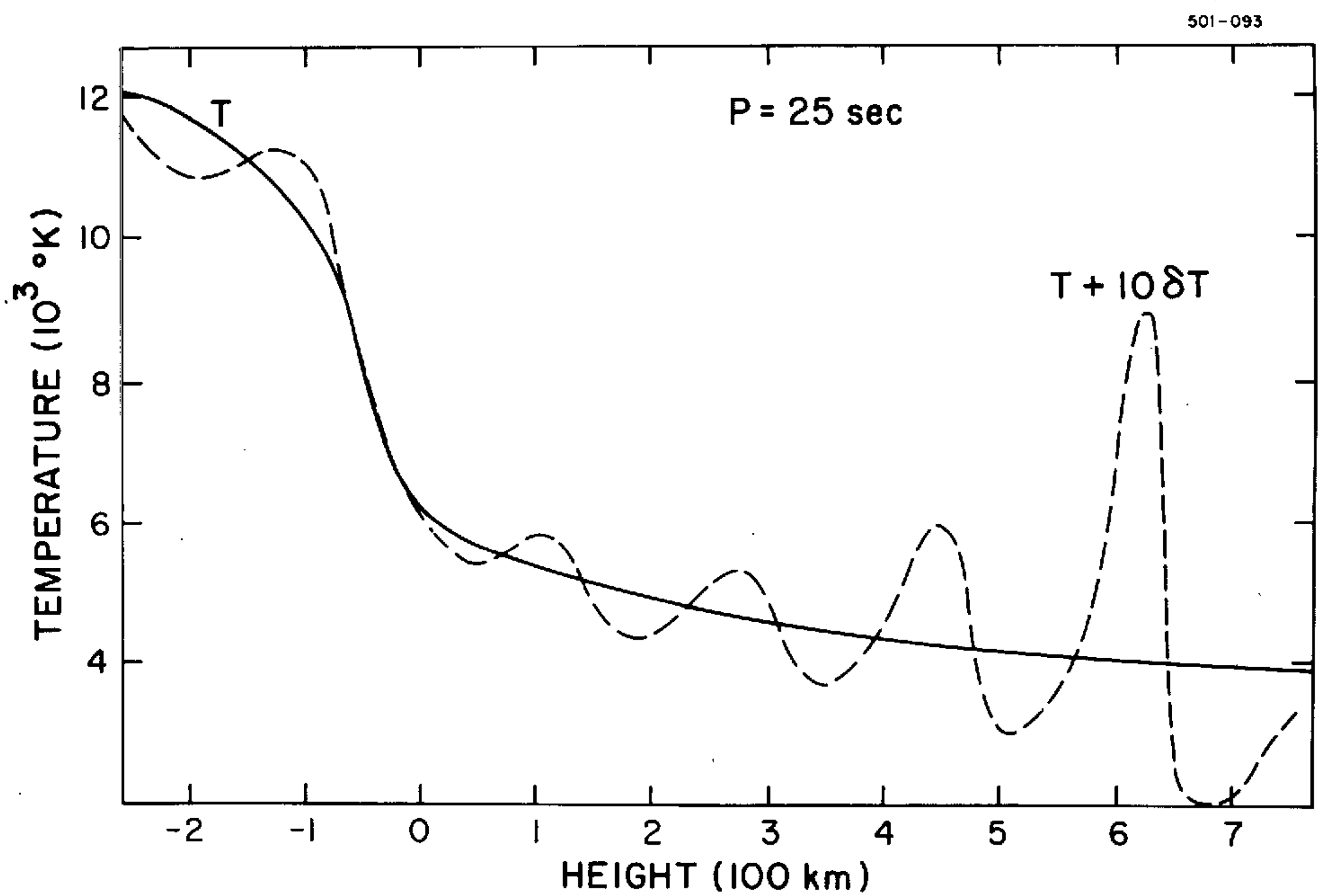

Figure 3. Temperature T and scaled temperature perturbation, $10^4\ \delta T$, as functions of height.

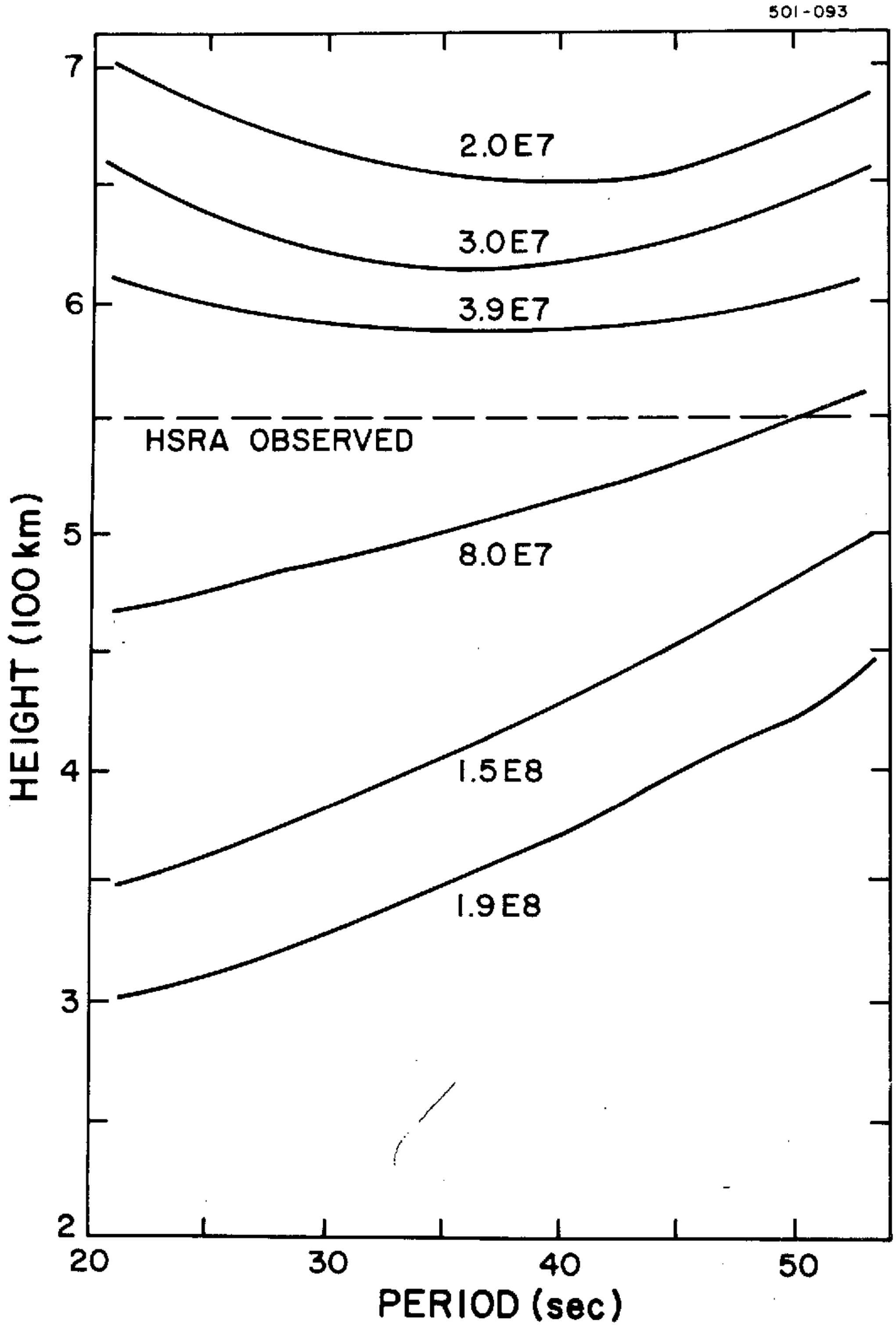

Figure 4. Height of shock formation as a function of wave period and initial energy flux.

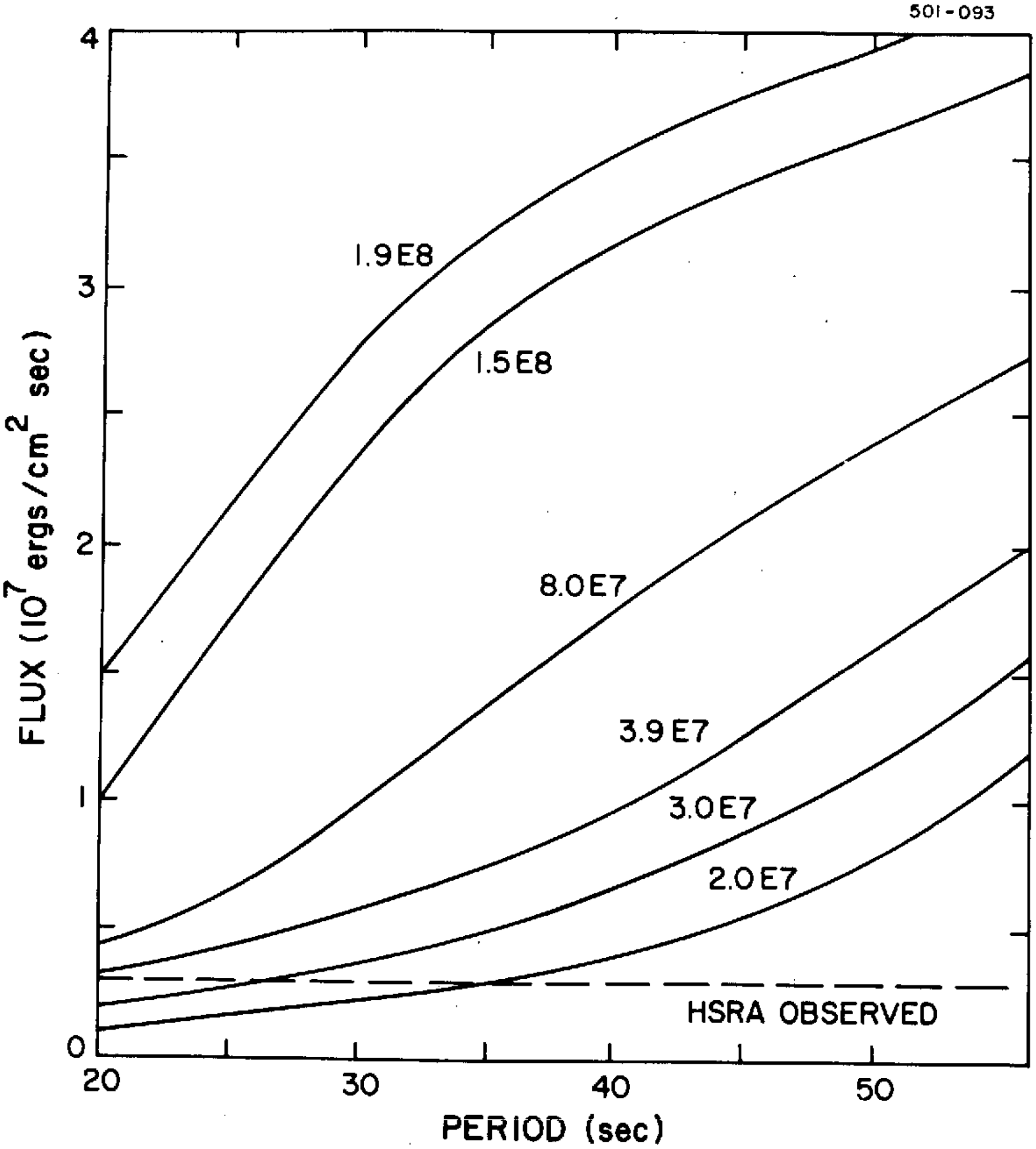

Figure 5. Energy flux carried beyond the shock as a function of wave period and initial energy flux.

The main limitation of this work is that we have used only a single wave. Calculation with several waves should give only minor changes in the main conclusions, however, since most of the energy is transported in waves with periods not very different from the ones we used.

CONCLUSION

The low chromosphere is heated by short-period waves. In a calculation with a single wave with a period of 30 sec and an initial energy flux of 3×10^7 ergs/cm^2 sec, the wave dissipates most of the energy at a height (h = 650 km) that agrees with the observed location of the temperature minimum, and the energy flux (3×10^6 ergs/cm^2 sec) that remains in the wave beyond the shock is sufficient to account for the radiative losses of the chromosphere.

REFERENCES

Athay, R. G., 1970, Astrophys. J., **161**, 713.

Biermann, L., 1946, Die Naturwissenschaften, **2**, 118.

__________. 1948, Zeits. f. Astrophys., **25**, 161.

Gingerich, O., R. W. Noyes, W. Kalkofen, and Y. Cuny, 1971, Solar Phys., **18**, 347.

Kurucz, R. L., 1974, Solar Phys., **34**, 17.

Osterbrock, D. E., 1961, Astrophys. J., **134**, 347.

Schwarzschild, M., 1948, Astrophys. J., **107**, 1.

Stein, R. F., 1968, Astrophys. J., **154**, 297.

Ulmschneider, P., 1970, Solar Phys., **12**, 403.

APPENDIX B

FORMATION OF THE SOLAR EUV SPECTRUM

Eugene H. Avrett

Center for Astrophysics
Harvard College Observatory and Smithsonian Astrophysical Observatory
Cambridge, Massachusetts 02138

Presented at
the Fifth Meeting of the Solar Physics Division
American Astronomical Society
January 19–23, 1975
University of Colorado, Boulder, Colorado

FORMATION OF THE SOLAR EUV SPECTRUM

Eugene H. Avrett

This is a brief progress report on work in progress with J. E. Vernazza and R. Loeser on the determination of empirical chromospheric models.

Figure 1 shows a theoretically determined continuum-intensity distribution at the center of the solar disk in the range 1300 to 100 Å. This region is filled with emission lines, particularly in the wavelength regions longward of the indicated absorption edges. Only three emission lines are shown: the 304 Å He II line, the 584 He I line, and Ly α. The insert shows the central part of the Ly α profile.

In this brief report I will discuss only the continuum-intensity distribution, showing where in the atmosphere various spectral features originate, and how the spectrum is formed at those depths. The object of this work is to determine a temperature stratification, by use of a non-LTE model atmosphere in hydrostatic equilibrium, so that the computed spectrum agrees as well as possible with the observed one. After such a model is established for a particular type of solar region or structure, we can calculate the radiative and conductive contributions to the chromospheric energy balance.

Before discussing the model, some comments should be made about how these computed results agree with observations. The computed intensity at 1300 Å and the Ly α wings agree reasonably well with the observed intensities, but the Ly α central reversal is too deep. The computed C I ground state continuum at 1100 Å is about a factor of 2 brighter than observed. The hydrogen Lyman continuum is in good agreement with the observations from 912 Å to about 700 Å. The He I 504 Å continuum agrees approximately with quiet sun observations or is slightly higher. The calculated He II continuum is too bright, perhaps by a factor of 5 or more, but our He II calculations are very preliminary and have not yet been examined carefully.

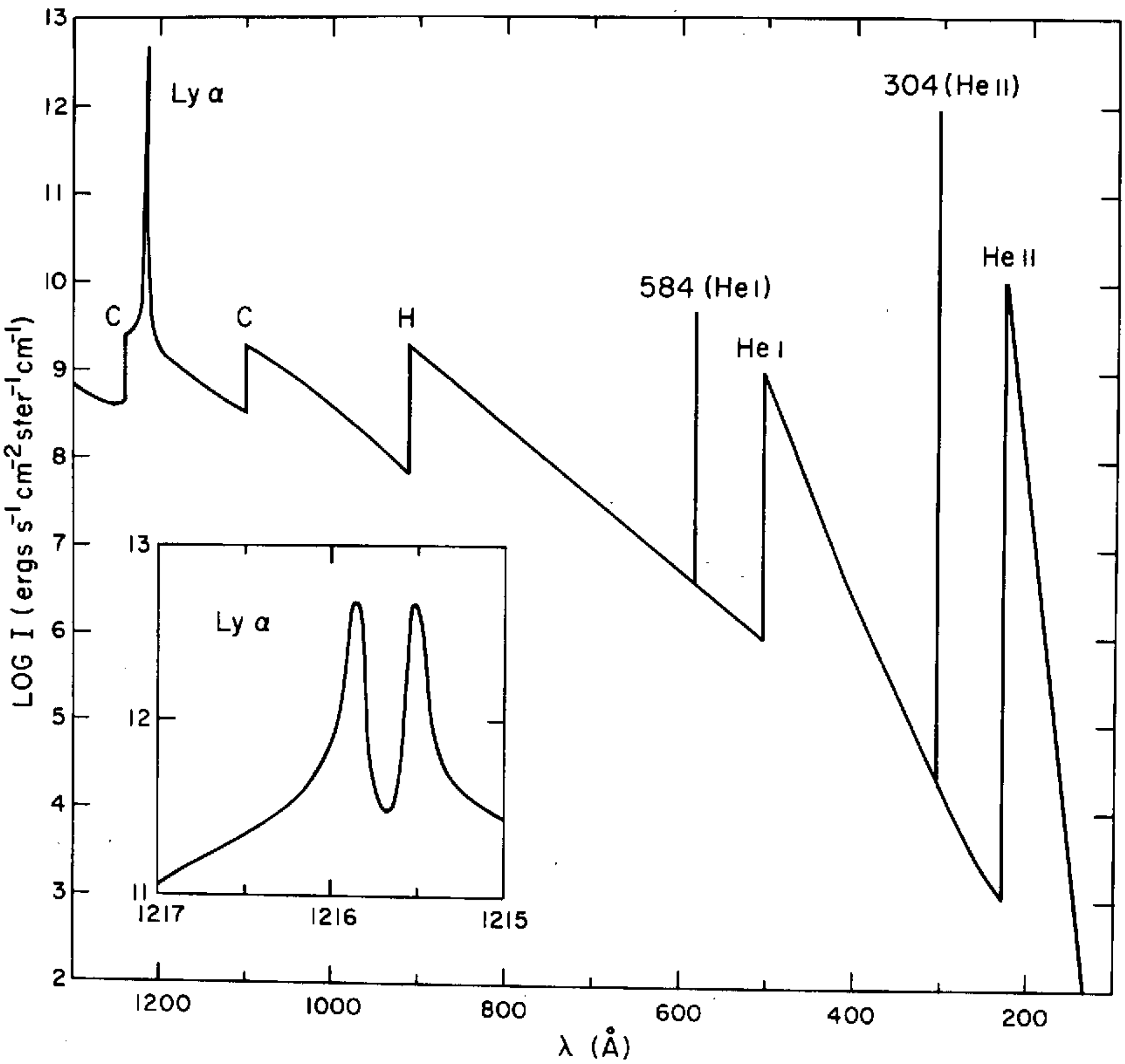

Ly α
304 (He II)
He II
584 (He I)
He I
C
C
H
Ly α
LOG I (ergs s^{-1} cm^{-2} ster^{-1} cm^{-1})
λ (Å)

Figure 1.

We are still in the process of adjusting the chromospheric model to match the observations, after having recently established a new model of the underlying photosphere and temperature minimum region (Vernazza, Avrett, and Loeser, 1975).

Figure 2 shows the temperature distribution that was used to obtain these results. The temperature minimum of about 4200 K appears at the extreme right. The middle chromosphere is characterized by a broad temperature plateau at about 6500 K, between 1000 and 2000 km. These are heights above $\tau = 1$ at 5000 Å in the photosphere. In the transition region between the chromosphere and corona we have introduced a 20, 000 K temperature plateau in order to account for reversals in the higher Lyman lines and for the slope of the Lyman continuum.

Figure 3 shows details of the intensity calculation at 1300 Å (or 0. 13 μm). Here, τ is the monochromatic optical depth at this wavelength. dI/dh (on a linear scale not shown) is the contribution per unit height to the intensity I at $\mu = 1$, which at this wavelength is formed between the temperature minimum and the 6500° plateau. B is the Planck function, S^{ab} is the continuum source function before scattering is taken into account, and S^{c} is the source function after the scattering correction. J is the mean intensity. The scale on the left of the source function graph is the intensity in units of ergs cm^{-2} s^{-1} st^{-1} Hz^{-1}. The corresponding brightness temperatures are shown on the right. The upper left panel shows the relative contributions to the absorption coefficient while the lower left panel shows the relative contributions to the emission coefficient. The dominant processes are Si I, C I, and absorption and scattering in the Ly α wing. The extreme departures from LTE are indicated in the right-hand panel by the differences between source function and Planck function.

Figure 4 shows the corresponding results at 1238 Å in the far wing of Ly α. The place of formation is now at a greater height than before, and becomes much higher in the atmosphere as we approach line center.

Figure 5 shows the results at the head of the 1100 Å carbon continuum. As noted above this computed intensity is about a factor of 2 higher than observed. We can determine from this diagram where and by how much the temperature should be lowered to get a better result.

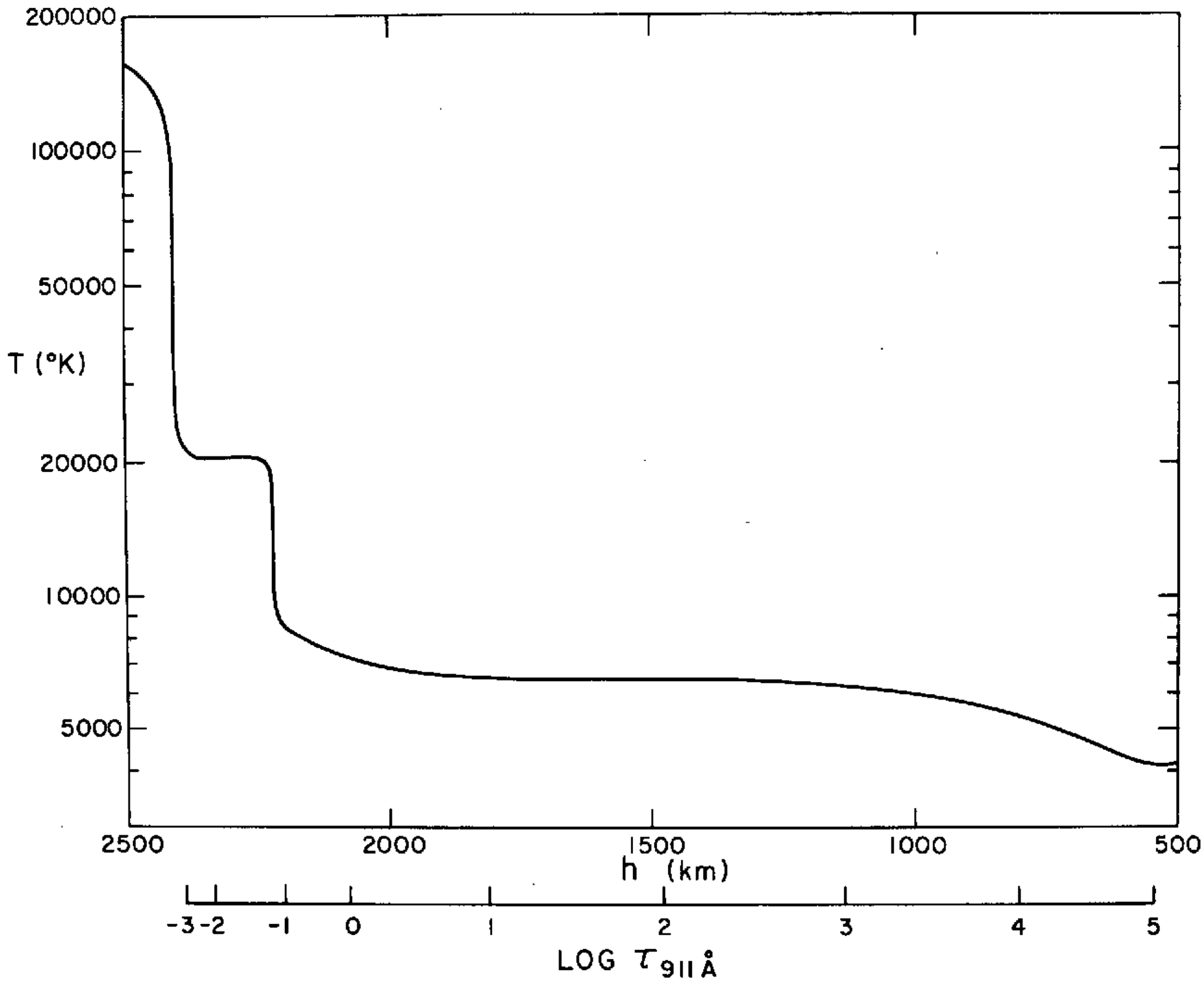
200000
100000
50000
T (°K)
20000
10000
5000
2500
2000
1500
1000
500
h (km)
-3 -2
-1
0
1
2
3
4
5
LOG $\tau_{911 Å}$

Figure 2.

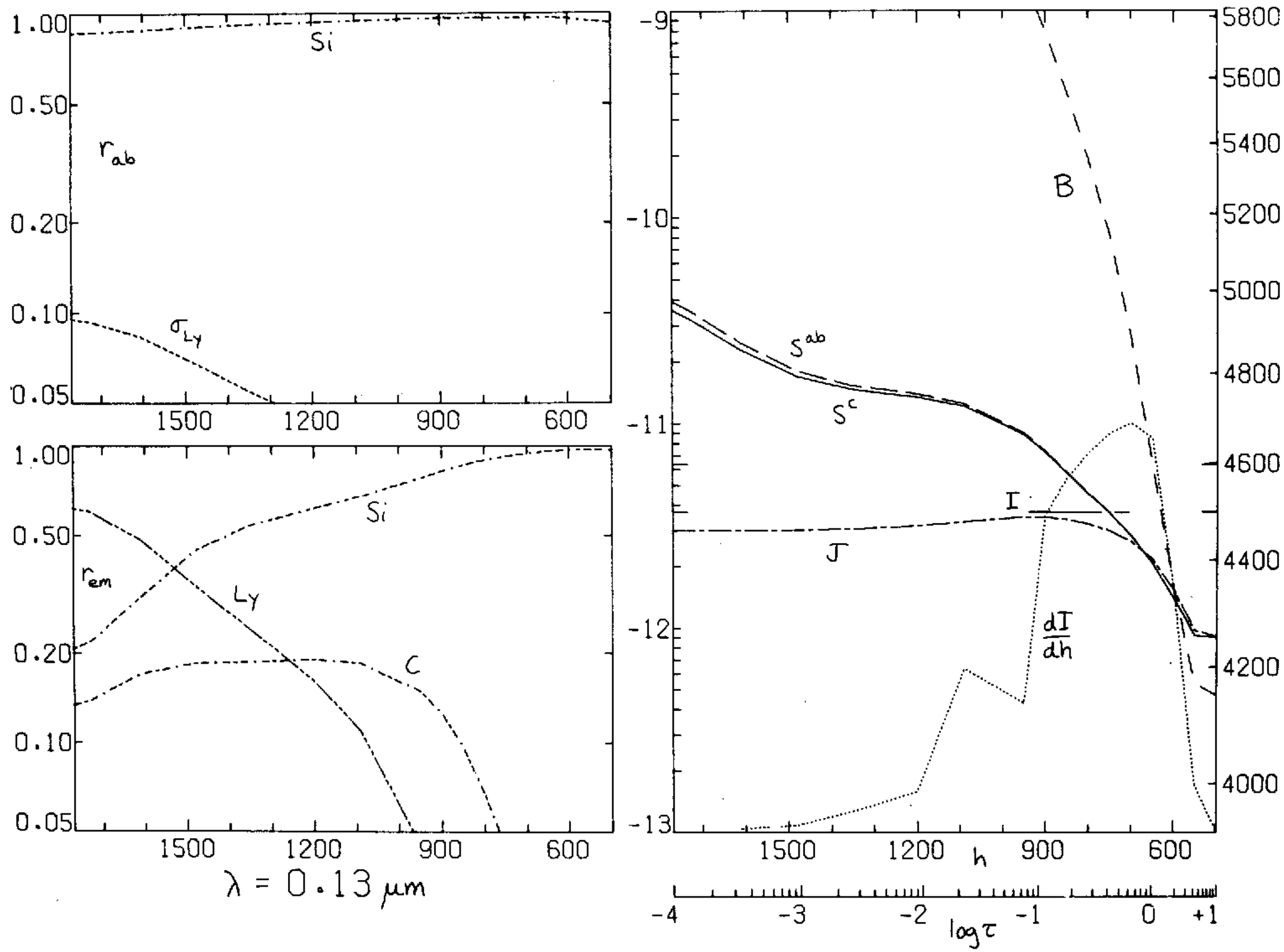
1.00
0.50
0.20
0.10
0.05
Si
r_{ab}
σ_{Ly}
1500
1200
900
600
r_{em}
Ly
C
$\lambda = 0.13\ \mu m$
-9
-10
-11
-12
-13
5800
5600
5400
5200
5000
4800
4600
4400
4200
4000
B
S^{ab}
S^{c}
I
J
$\frac{dI}{dh}$
h
-4
-3
-2
-1
0
+1
log τ

Figure 3.

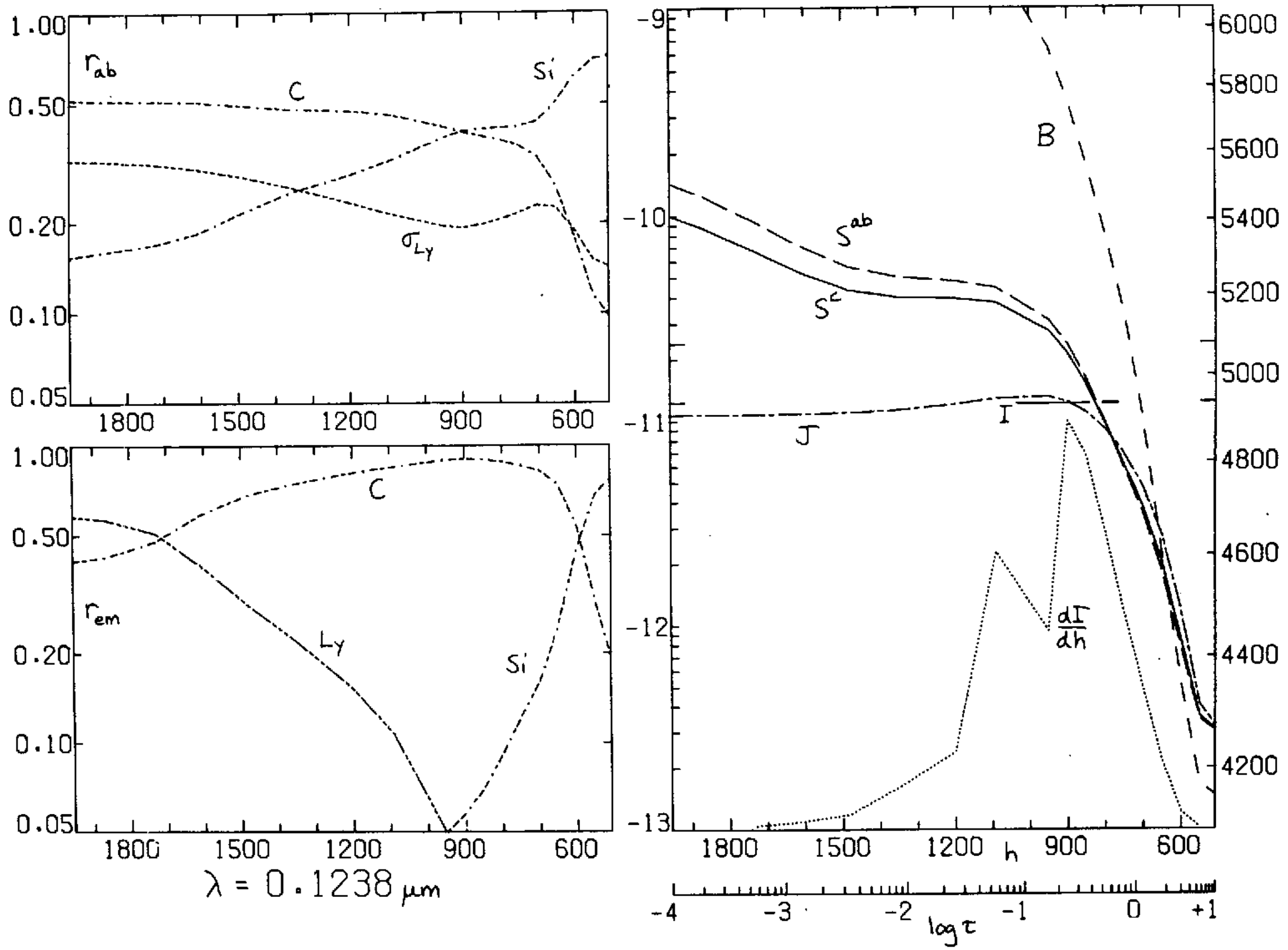

1.00
0.50
0.20
0.10
0.05
r_{ab}
C
Si
$\sigma_{L\gamma}$
1800
1500
1200
900
600
r_{em}
C
$L\gamma$
Si
λ = 0.1238 μm
-9
-10
-11
-12
-13
B
S^{ab}
S^{c}
J
I
$\frac{dI}{dh}$
h
6000
5800
5600
5400
5200
5000
4800
4600
4400
4200
-4
-3
-2
-1
0
+1
log τ

Figure 4.

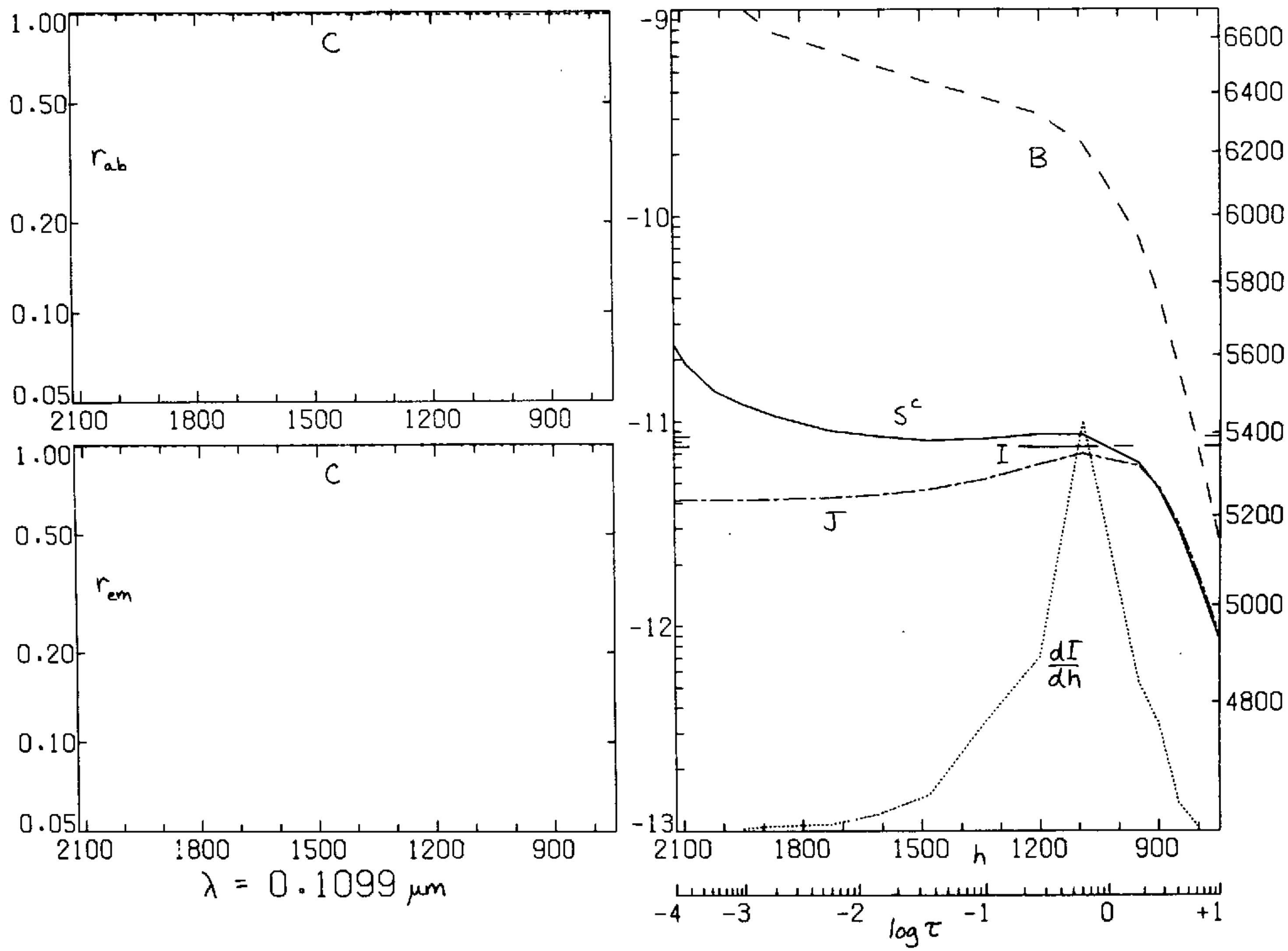
1.00
0.50
0.20
0.10
0.05
C
r_{ab}
2100
1800
1500
1200
900
r_{em}
λ = 0.1099 μm
-9
-10
-11
-12
-13
6600
6400
6200
6000
5800
5600
5400
5200
5000
4800
B
S^c
I
J
$\frac{dI}{dh}$
h
-4
-3
-2
-1
0
+1
log τ

Figure 5.

Figure 6 shows that the head of the Lyman continuum is formed at the other end of the 6500° plateau at the base of the transition region between chromosphere and corona. (The sharp variations in dI/dh and S^c do not have any particular significance and should become smoother when more depth points are added.)

The higher temperature layers in the transition region become important at shorter wavelengths in the Lyman continuum, as shown in Figure 7. Here at 700 Å the contribution of the 20,000° region between $\tau = 10^{-3}$ and 10^{-1} is greater than the contribution closer to $\tau = 1$. There is even a small contribution from yet higher temperature layers where τ is less than 10^{-3}. This is an extreme example of the failure of the Eddington–Barbier relation.

Figure 8 shows that the conditions at the head of the He I 504 Å continuum are strikingly different from those in the Lyman continuum. We have introduced an incident radiation field due to the various coronal emission lines, the strongest being the 304 Å line of He II. The coronal radiation penetrates into the upper chromosphere causing He I ionization and excitation in a region where the temperature is 7000°. A local maximum occurs in the D_3 and 10830 line opacities at around 2000 km. Reduced incident coronal radiation removes this extra component of absorption. As a consequence, these lines should be weaker, as they are observed to be, in the presence of coronal holes, as has been discussed in other papers at this meeting.

Within the coming months we expect to complete a detailed study of the C I, H, He I, and He II continua and the H and He lines, and to establish the temperature and density stratification of quiet and active regions with different amounts of incident coronal line radiation. For each of these models we will determine the radiative and conductive contributions to the chromospheric energy balance.

REFERENCE

Vernazza, J. E., Avrett, E. H., and Loeser, R., 1975, Astrophys. J. Suppl. (in press).

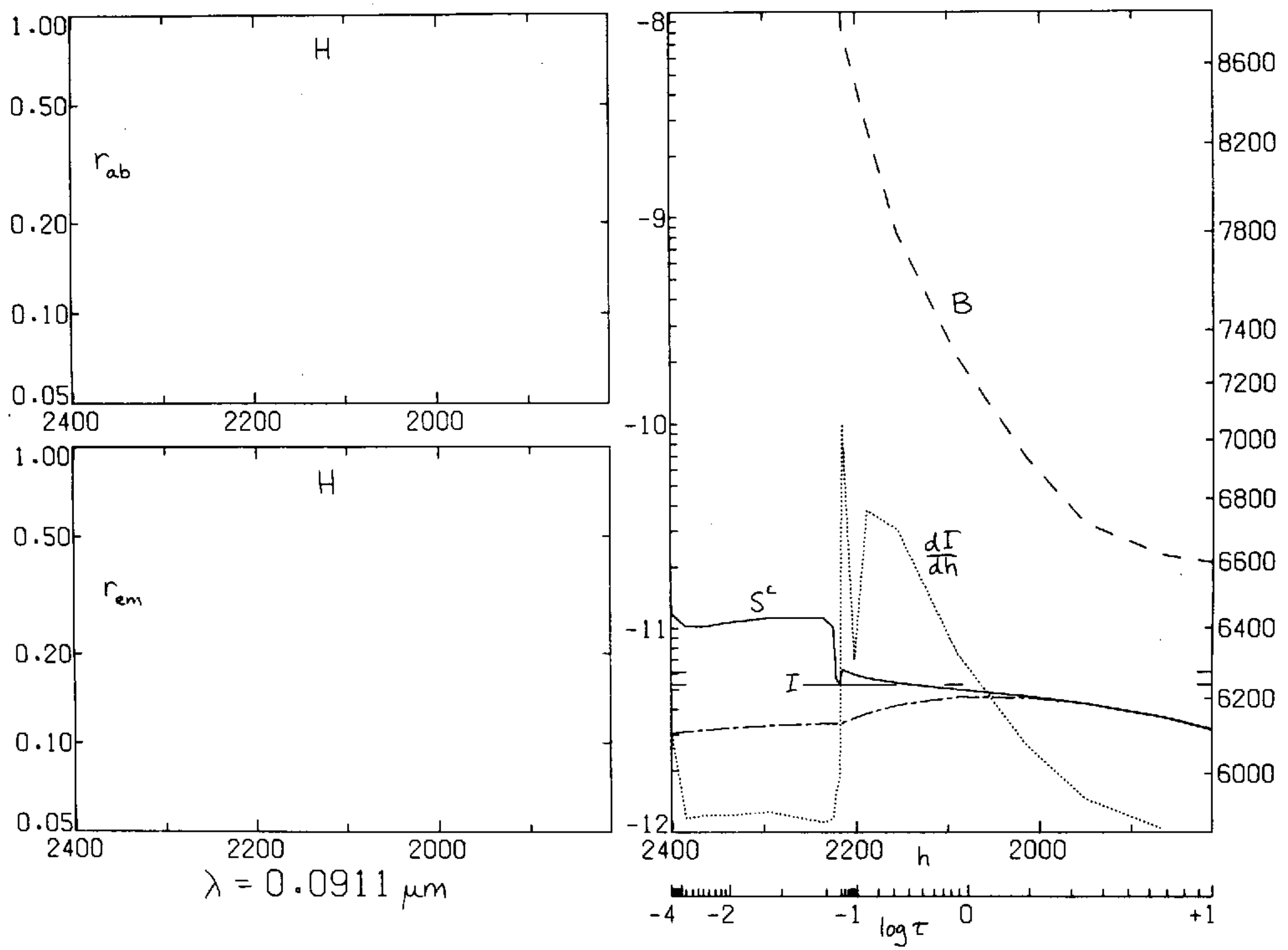
H
1.00
0.50
r_{ab}
0.20
0.10
0.05
2400
2200
2000
H
1.00
0.50
r_{em}
0.20
0.10
0.05
2400
2200
2000
$\lambda = 0.0911\ \mu m$
-8
-9
-10
-11
-12
8600
8200
7800
7400
7200
7000
6800
6600
6400
6200
6000
B
$\frac{dI}{dh}$
S^c
I
2400
2200
h
2000
-4
-2
-1
$\log \tau$
0
+1

Figure 6.

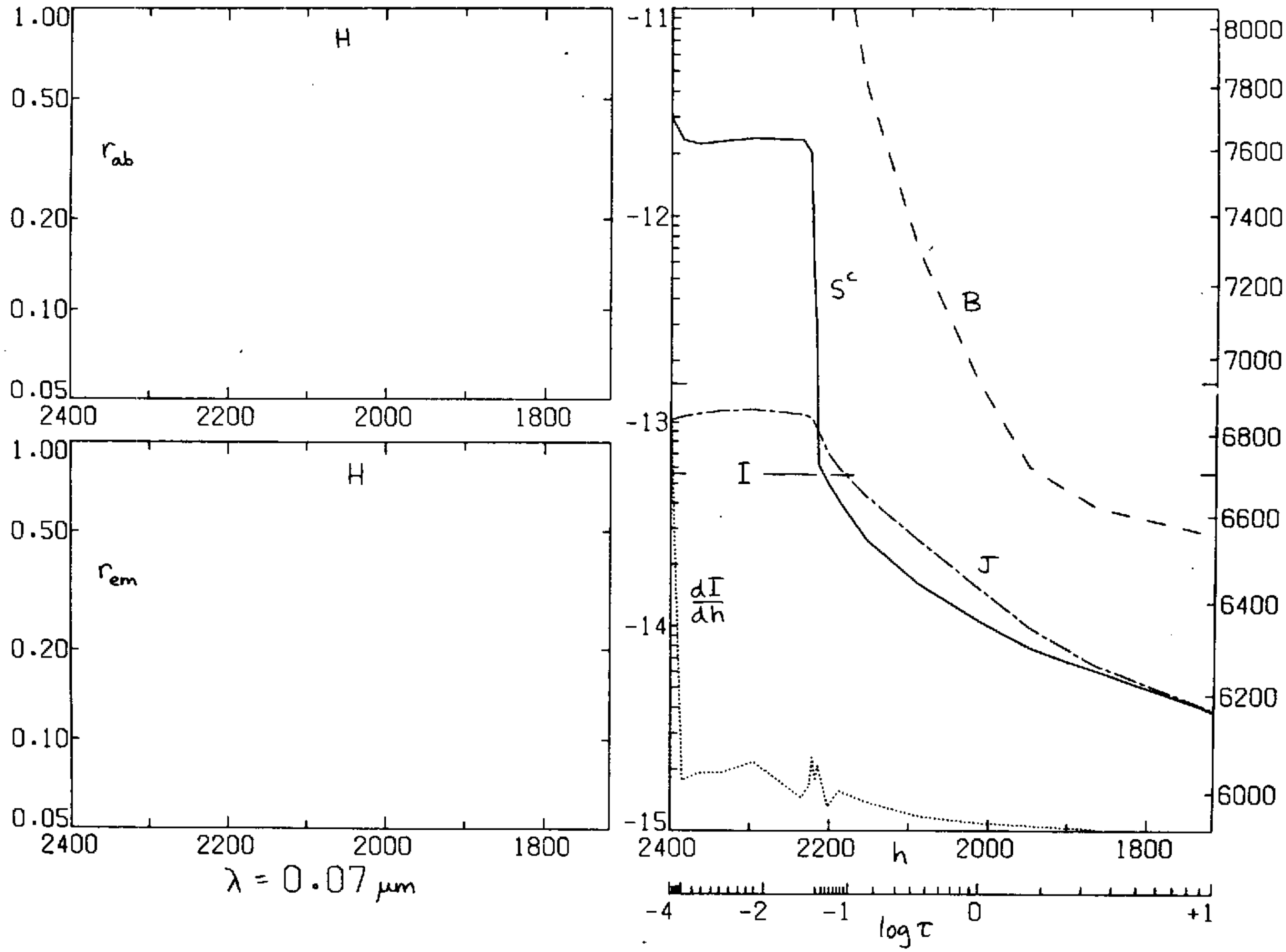
H
r_{ab}
1.00
0.50
0.20
0.10
0.05
2400
2200
2000
1800
H
r_{em}
1.00
0.50
0.20
0.10
0.05
2400
2200
2000
1800
λ = 0.07 μm
-11
-12
-13
-14
-15
8000
7800
7600
7400
7200
7000
6800
6600
6400
6200
6000
S^c
B
I
J
$\frac{dI}{dh}$
2400
2200
h
2000
1800
-4
-2
-1
0
+1
log τ

Figure 7.

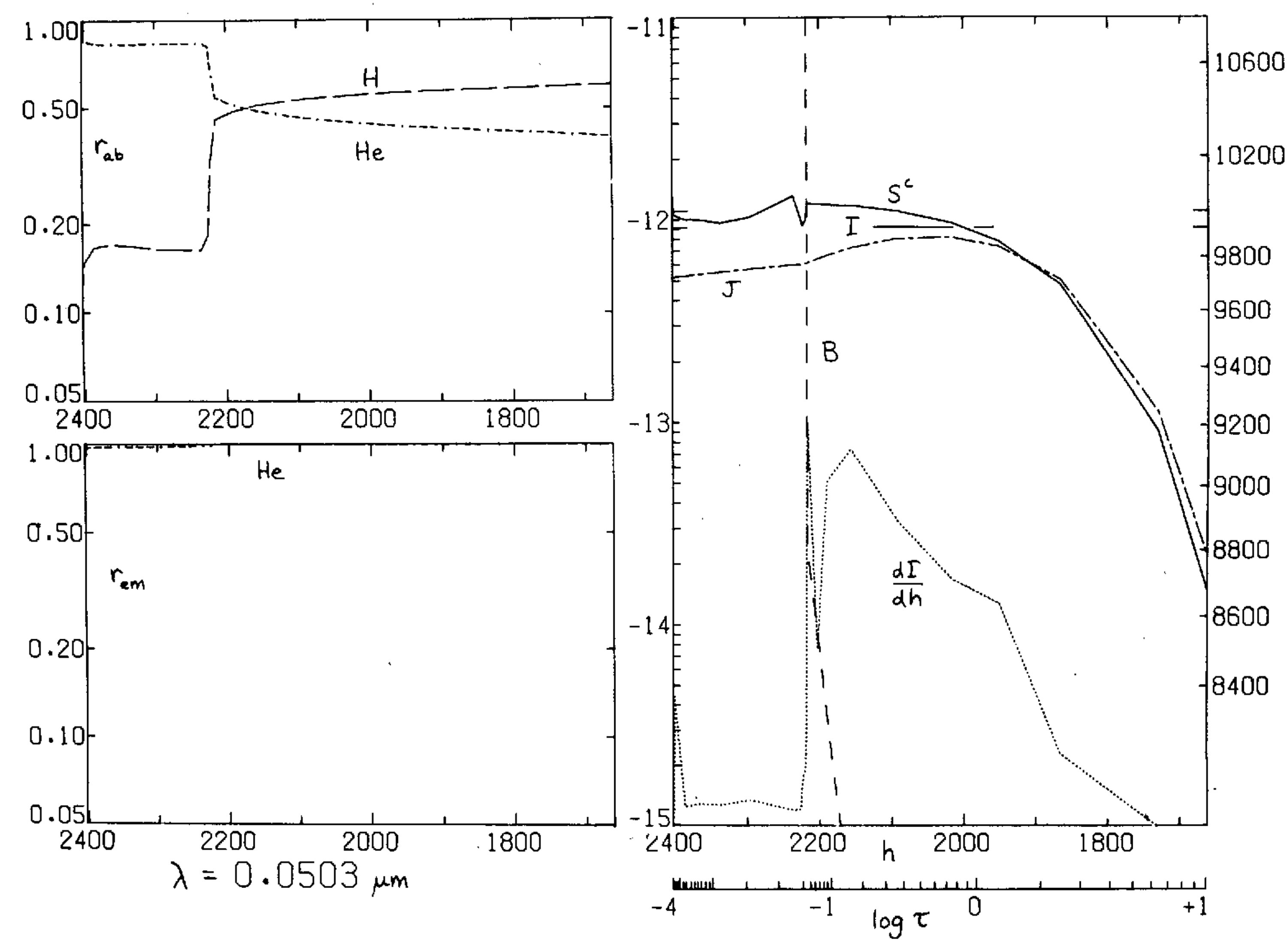
1.00
0.50
0.20
0.10
0.05
r_{ab}
H
He
2400
2200
2000
1800
r_{em}
$\lambda = 0.0503\ \mu m$
-11
-12
-13
-14
-15
10600
10200
9800
9600
9400
9200
9000
8800
8600
8400
S^c
I
J
B
$\frac{dI}{dh}$
h
-4
-1
0
+1
log τ

Figure 8.